Photometric redshift outliers and their impact on LSST weak lensing cosmology: Insights from a Gaussian island model

By

Jonah Lotz

_____

A Thesis Submitted to The W.A. Franke Honors College

In Partial Fulfillment of the bachelor's degree
With Honors in

Astronomy

THE UNIVERSITY OF ARIZONA

D E C E M B E R 2 0 2 4

Approved by:

Dr. Tim Eifler
Department of Astronomy

Photometric redshift outliers and their impact on LSST weak lensing cosmology: Insights from a Gaussian island model

Jonah Lotz,[1,2] Supranta S. Boruah,[1,3] and Tim Eifler[1,4]

[1] *Department of Astronomy and Steward Observatory, The University of Arizona, 933 North Cherry Avenue, Tucson, AZ 85721, USA*
[2] *Department of Computer Science, The University of Arizona, 1040 E 4th Street, Tucson, AZ 85721, USA*
[3] *The Center for Particle Cosmology, University of Pennsylvania, 209 S 33rd Street, Philadelphia, PA 19104, USA*
[4] *Department of Physics, The University of Arizona, 1118 E 4th Street, Tucson, AZ 85721, USA*

Abstract

Next-generation cosmological surveys, such as the Vera C. Rubin Observatory's Legacy Survey of Space and Time (LSST), will deliver unprecedented statistical power to probe fundamental aspects of the Universe, including the nature of dark energy and dark matter. However, achieving this precision requires careful control of systematic uncertainties. One critical challenge is the presence of catastrophic photometric redshift (photo-z) outliers - galaxies for which the photometric redshift estimate deviates substantially from the true (spectroscopic) redshift. These outliers can skew the inferred redshift distributions used in weak lensing analyses, biasing constraints on cosmological parameters. We investigate how catastrophic photo-z outliers affect key cosmological parameters derived from LSST-like weak lensing data. Using a "Gaussian Island Model" to represent these outliers as distinct islands in redshift space, we find that even small fractions of certain outlier populations can significantly bias constraints on matter density (Ω_m), time evolution of dark energy (w), and the amplitude of matter fluctuations (S_8). Our analysis shows that "false low-z" outliers (high z, low z_{ph}) induce more pronounced biases than "false high-z" galaxies (low z, high z_{ph}), making accurate estimates of the false low-z outlier fraction especially critical. This sensitivity underscores the need for careful outlier characterization, improved photo-z calibration, and strategic spectroscopic follow-up. By better understanding and mitigating these catastrophic outliers, we can preserve the integrity of cosmological inferences and fully exploit the scientific potential of next-generation weak lensing surveys.

1. INTRODUCTION

1.1. *Next Generation Surveys*

Next-generation Stage-IV surveys, such as the Dark Energy Spectroscopic Instrument (DESI; DESI Collaboration et al. 2016), the Nancy G. Roman Space Telescope (NGRST; Spergel et al. 2015), and the Vera C. Rubin Observatory's Legacy Survey of Space and Time (LSST; Ivezić et al. 2019), mark a pivotal era in observational cosmology. By offering unprecedented precision and scale, these surveys are poised to enhance our understanding of the Universe's large-scale structure and constrain fundamental cosmological parameters, including the nature of dark energy and dark matter.

Among these cutting-edge surveys, this thesis focuses on LSST's weak lensing program, which is discussed further in Section 1.2. The telescope for this survey, the Simonyi Survey Telescope, boasts an 8.4-meter aperture with a 9.6-deg^2 field of view (Ivezić et al. 2019). This is accomplished through a novel three-mirror design, characterized as a modified Paul-Baker Mersenne Schmidt system shown in Figure 1. This design allows for an image quality of better than 0.3 arcseconds for all bands. A pivotal component of the Simonyi Survey Telescope is its state-of-the-art camera, recognized as the largest digital camera ever constructed for an astronomical survey. The camera features an impressive 3.2 gigapixels, compromised of 189 4K x 4K CCD sensors. This immense pixel count enables LSST's expansive 9.6-deg^2 field of view and the need to achieve 0.2" x 0.2" pixels for optimal sampling in the anticipated seeing conditions (Ivezić et al. 2019).

Using this equipment, LSST is guided by an ambitious and multifaceted scientific agenda, centered around a core set of primary themes (Ivezić et al. 2019):

I. Investigating the nature of dark energy and dark matter.

II. Cataloging objects within our solar system.

III. Detecting and characterizing transient and variable phenomena.

IV. Charting the structure and dynamics of the Milky Way.

1.2. *Weak Lensing*

One of the most powerful tools in cosmology is the use of weak gravitational lensing, often referred to simply as weak lensing. This phenomenon involves the slight distortion of images of distant galaxies caused by the gravitational pull of matter located between the observer and

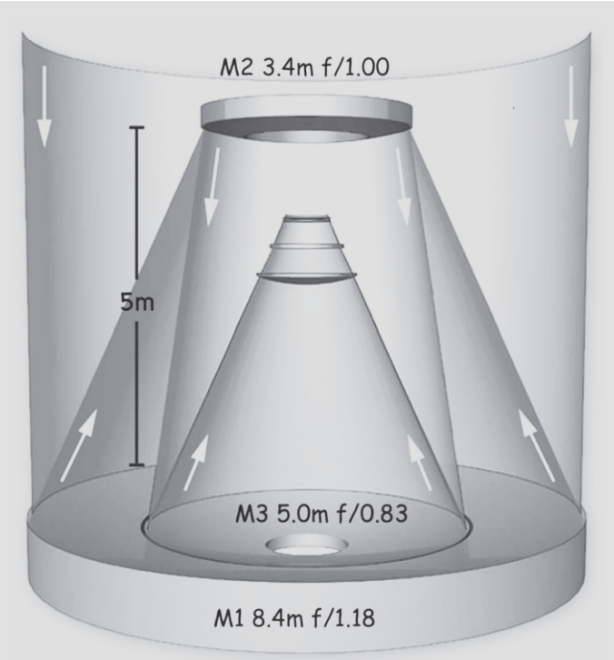

Figure 1. The three-mirror design of the Simonyi Survey Telescope. It features a unique monolithic mirror, with the primary and tertiary mirrors seamlessly integrated into a continuous compound surface. Adapted from Ivezić et al. (2019).

the source galaxies (Abdalla et al. 2022). These distortions manifest as coherent alignments in the shapes of background galaxies, which appear slightly stretched or sheared.

Weak lensing is quantitatively described by three parameters: shear (γ_1, γ_2) and convergence (κ). The shear parameters measure the anisotropic stretching of galaxy images, effectively distorting them into more or less elliptical shapes. Specifically, the observed ellipticity is the combination of two quantities: gravitational shear and intrinsic ellipticity (Mandelbaum 2018). Gravitational shear is the primary signal of interest, caused by the distortion of light from background galaxies. On the other hand, convergence (κ) relates to the isotropic magnification and distortion of the image size and brightness, providing information about the projected mass density along the line of sight (Abdalla et al. 2022).

In the context of LSST, weak lensing is a critical probe for investigating the distribution of dark matter and the nature of dark energy. By measuring the shear, the projected mass distribution of the intervening large-scale structure can be reconstructed. This will allow LSST to map the distribution of dark matter in the universe (Ivezić et al. 2019). Additionally, weak lensing serves as one of LSST's five primary cosmological probes aimed at constraining the evolution of dark energy (The LSST Dark Energy Science Collaboration et al. 2018). Through precise measurements of the shear correlation functions and convergence power spectra across different redshift bins, weak lensing can provide stringent constraints on the equation of state of dark energy (w). This equation of state is parameterized by w_0 and w_a, which describe the relationship between dark energy pressure and density.

1.3. *Tension in S_8*

One of the most interesting hints for new physics in cosmology is the discrepancy between measurements of the matter clustering strength in the universe (Poulin et al. 2023).

A critical parameter in understanding the Universe's matter distribution is S_8, defined as

$$S_8 = \sigma_8 \sqrt{\frac{\Omega_m}{0.3}}, \tag{1}$$

where σ_8 is the standard deviation of matter density fluctuations in spheres of size 8 $h^{-1}Mpc$ and Ω_m represents the fractional energy density of matter.

This parameter provides insights into the clustering amplitude of matter in the universe and constraining it is one of the core goals of weak lensing. However, a persistent discrepancy, often referred to as the S_8 tension, has emerged in recent weak lensing surveys.

As Poulin et al. (2023) discuss, measurements of the distribution of galaxies and matter in the late Universe, obtained through probes like galaxy clustering and weak lensing, indicate a smoother distribution than predicted by the evolution of fluctuations observed in the Cosmic Microwave Background (CMB). Specifically, low-redshift probes consistently yield S_8 values 2σ lower than those derived from primary CMB anisotropies and the CMB lensing power spectrum. Two low-redshift surveys, DES and KiDS, have computed S_8 values significantly lower than the Planck CMB constraint (Abbott et al. 2022; Heymans, Catherine et al. 2021). While this discrepancy alone is not definitive, its persistent observation across multiple independent measurements suggests a potentially significant gap that could challenge our understanding of cosmic structure formation and evolution. The tension raises questions about the completeness of the standard (ΛCDM) cosmological model and the need for extensions or modifications.

One of the difficulties in measuring S_8 arises from its model dependence, as analyzed by Abdalla et al. (2022). The measurement of S_8 relies on assumptions about the underlying cosmological model - usually ΛCDM - meaning that varying other cosmological parameters can influence the derived S_8 constraints.

1.4. *Redshift Measurements*

As the universe undergoes continuous expansion, the wavelengths of electromagnetic radiation emitted by galaxies are stretched, resulting in a shift toward the red end of the spectrum - a phenomenon known as redshift. The degree of this wavelength stretching correlates directly with the object's recessional velocity and, consequently, its distance from us.

In the realm of weak lensing cosmology, precise redshift measurements are indispensable. Accurate redshift information is required for modeling the shear signal accurately, thereby enabling precise mapping of the large-scale structure of the universe and constraining cosmological models effectively (Abdalla et al. 2022).

There are two primary ways in which redshift can be measured. Spectroscopic redshift measurement involves the detailed analysis of a galaxy's spectrum to identify characteristic spectral features, such as emission or absorption lines. Due to the expansion-induced redshift, these spectral lines are shifted from their rest-frame wavelengths; by calculating the extent of this displacement, the redshift value can be computed. Alternatively, photometric redshift estimation leverages the galaxy's apparent brightness across multiple photometric bands (filters). Techniques such as template fitting, Bayesian inference, color-color diagram analysis, and machine learning algorithms are utilized to infer redshift values based on the observed photometric data (Mandelbaum 2018).

Spectroscopic redshifts are renowned for their high precision and are often regarded as the "true" redshift. However, obtaining spectroscopic data demands significant observational resources, including extensive telescope time and specialized instrumentation. In contrast, photometric redshifts offer a more economical and rapid alternative, enabling redshift estimation for vast numbers of galaxies. Unfortunately, this method compromises accuracy due to its reliance on limited photometric band information. Extreme cases of this inaccuracy are the focus of this paper and will be discussed further in Section 2.

2. CATASTROPHIC PHOTO-Z OUTLIERS

Photometric and spectroscopic redshift methods differ significantly in their levels of detail and precision, leading to potential discrepancies in their respective measurements. Specifically, photometric redshifts tend to broaden the redshift distribution, thereby contributing to these variances. Although the two methods generally correlate, there are instances where the differences between them are unexpectedly large. Such substantial discrepancies are referred to as catastrophic photometric redshift (photo-z) outliers. These outliers occur when a photometric redshift estimation significantly deviates from the more accurate spectroscopic redshift, undermining the reliability of the photometric method.

Figure 2 highlights the relationship between true and photometric redshifts of 178,269 galaxies in the LSST Y2 mock catalogue from Graham et al. (2018, 2020). More detail on this catalogue can be found in those papers, along with Fang et al. (2021). We note the significant portion of galaxies that deviate considerably from the diagonal. These galaxies, colored in red, make up the two islands of catastrophic outliers. The upper left island contains galaxies whose true redshift is significantly higher than the determined photometric redshift. The bottom right island is the opposite, with large photometric redshifts for nearby galaxies. Throughout the remainder of this thesis, these will be referred to as false low-z galaxies and false high-z galaxies, respectively.

2.1. *Causes for Catastrophic Photo-z Misestimation*

These outliers can arise from various factors, each contributing to the degradation of photo-z reliability.

Schaan et al. (2020) discuss several of these factors. The first is "type"-redshift degeneracy, where galaxies at different redshifts exhibit similar fluxes in observed photometric bands due to the limited number of features in their spectra. While this degeneracy can be mitigated by adding additional photometric bands to the datasets, this is not always possible and the degeneracy still poses a significant challenge to photo-z training. Additionally, the misidentification of two superimposed galaxies as a singular object leads to improper determinations of redshifts. This phenomenon, called blending, also leads to catastrophic outliers in algorithms that produce point estimates of redshifts (MacCrann et al. 2021).

Furthermore, photo-z algorithms, whether template-fitting or machine-learning-based, depend on accurate priors about the types and redshifts of galaxies in the sample. Inaccuracies in these priors, often derived from spectroscopic data, can lead to biased photo-z estimates Mandelbaum (2018). However, constructing such priors is difficult, as spectroscopy at the required depth is limited to small sub-samples. To ensure that the priors are accurate and do not create bias in the photo-z, spectroscopic follow-ups over large portions of the sky are needed.

Finally, Bernstein & Huterer (2010) examine several more factors. They find that the specific photo-z algorithm can lead to variations in outlier rates. For instance, an algorithm that does not contain a magnitude prior may be more prone to catastrophic outliers. Additionally, they discuss how certain spectral features can

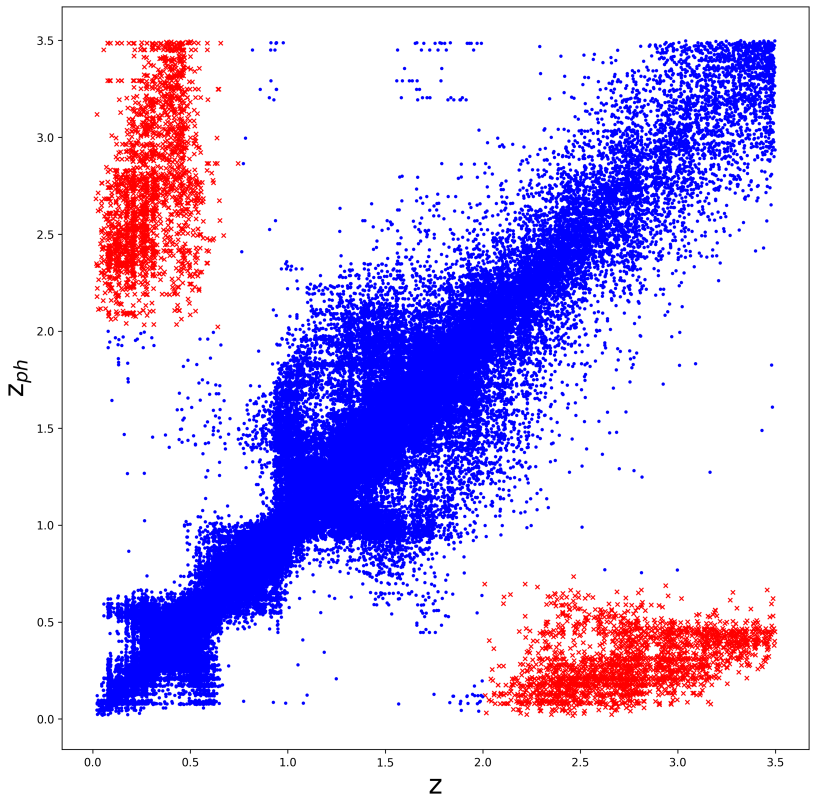

Figure 2. The mock galaxy catalogue used for photo-z studies of LSST Year 2, as described in Graham et al. (2018, 2020), provides a simulated dataset for analyzing photo-z outliers. The catalogue includes both the true redshifts z and the photometric redshifts z_{ph} for a sample of 178,269 galaxies. The red x-marks indicate catastrophic outliers, representing two islands in the top left and bottom right.

be mistaken for others at different redshifts, leading to large redshift misestimations. An example mentioned by Sun et al. (2009) is that high-redshift Lyman breaks can be confused with low-redshift 400 nm breaks. They analyze a specific case where a 1% fraction of galaxies at a true redshift of 0.4 are misidentified as being at a photometric redshift of 3.5 due to this confusion. This type of catastrophic redshift error can severely bias the results of cosmological analyses based on weak lensing measurements.

2.2. *Photo-z Outlier Challenges*

As Bernstein & Huterer (2010) analyzed, catastrophic photo-z errors can severely bias estimates of cosmological parameters derived from weak lensing surveys. These outliers distort the inferred redshift distribution of galaxies, which is crucial for accurately measuring the lensing signal and interpreting cosmological parameters such as the dark energy equation of state parameters w_0 and w_a, neutrino mass, M_ν, and curvature, Ω_k.

While the presence of these outliers is generally acknowledged, the precise outlier fraction often remains unknown due to the cost of spectral measurements discussed in Section 1.4. This lack of knowledge poses a critical challenge because accurately quantifying outlier fractions is essential for mitigating their impact on cosmological parameter estimation (Fang et al. 2021). For instance, Schaan et al. (2020) highlight that to avoid a 1σ bias in the dark energy equation of state parameters, the outlier fractions need to be known to within 5% of their values. Without a clear understanding of the outlier fraction, it becomes difficult to disentangle the genuine cosmological signal from the spurious effects introduced by misclassified galaxies.

Furthermore, Bernstein & Huterer (2010) find that a spectroscopic-redshift failure rate of less than 0.15% is needed to avoid substantial biases in cosmological parameter estimation. This rate - the percentage of objects for which spectroscopic samples fail to produce a reliable redshift measurement - can significantly contribute to the formation of catastrophic outliers. A spectroscopic survey with approximately 1 million redshifts would be required for a high-redshift study such as LSST to reach such a low rate Bernstein & Huterer (2010). This poses a logistical and financial challenge, especially given the many galaxies targeted in these large-scale sur-

veys. Spectroscopic redshifts are too costly and time-consuming to acquire in such large quantities.

2.3. *Gaussian Island Model*

Since it is difficult to determine the exact outlier fraction, we should adopt a flexible scheme to model the photo-z outliers in the data. To do this, we propose a "Gaussian Island Model" as the primary framework for our analyses. This model offers a modular and flexible approach to characterizing outlier populations, enabling the identification and treatment of distinct regions in the redshift parameter space where significant deviations between photometric and spectroscopic redshifts occur. This model operates under two key assumptions:

I. All outliers are contained within 2 islands where one island has $z < 0.75$ and $z_{ph} > 2.0$ and the other has $z > 2.0$ and $z_{ph} < 0.75$.

II. Each island is described by a Gaussian mixture model, delineated by the variables redshift (z) and photometric redshift (z_{ph}).

This model is detailed further in 3.3. The first assumption was derived from a similar model by Fang et al. (2021) that uses an "island model". However, they assume a uniform true redshift distribution for a given photo-z. We believe a Gaussian mixture model approach is another effective methodology. By assuming this distribution for each island, we achieve precise modeling of the distribution within each outlier region and gain enhanced flexibility through the straightforward manipulation of Gaussian parameters.

3. LSST-Y1 SURVEY & MODELING

3.1. *Survey Assumptions & Choices*

In this study, we base our LSST-Y1 survey assumptions on the guidelines provided in the DESC Science Requirement Document (SRD; The LSST Dark Energy Science Collaboration et al. 2018.) The simulated LSST-Y1 survey spans an area of 12,300 square degrees. We model the redshift distributions for both source and lens galaxy samples using the Smail distribution (Smail et al. 1995), characterized by $n(z) \propto z^2 \exp\left[-\left(\frac{z}{z_0}\right)^{\alpha}\right]$. We add outliers to this $n(z)$, the form of which is discussed in Section 3.3.

For the source galaxies, we adopt Smail distribution parameters of $z_0 = 0.191$ and $\alpha = 0.870$ as specified in Fang et al. (2020), resulting in an effective number density of $n_{\rm eff} = 11.2$ galaxies per square arcminute. The source sample is divided into five tomographic redshift bins.

We compute the angular shear correlation functions across 26 logarithmically spaced angular bins ranging from 2.5 to 900 arcminutes. To address potential inaccuracies in theoretical models at small scales, we implement angular scale cuts. Following Fang et al. (2020), we use angular scale cuts of $\theta > [80.88', 54.19', 42.85', 35.43', 29.73']$. For cosmic shear measurements, we impose a multipole cut-off at $\ell_{\rm max} = 3000$ (Fang et al. 2020).

3.2. *Modeling*

In this section, we describe how we model various systematic effects in our theoretical data vectors. We note that baryonic effects are not included in our analysis, as we assume their influence is minimal within the scales considered.

While cosmic shear analyses typically assume that galaxies are randomly oriented, galaxies can exhibit correlated orientations due to the influence of the surrounding dark matter structures (Mandelbaum 2018). To account for this intrinsic alignment (IA) in our data vectors, we employ the non-linear alignment (NLA) model proposed by Bridle & King (2007). Within the NLA framework, the redshift-dependent amplitude of the IA signal is defined as:

$$A_{\rm IA}(z) = -a_{\rm IA}\,\frac{C_1\,\rho_{\rm cr}\,\Omega_{\rm m}}{G(z)}\left(\frac{1+z}{1+z_0}\right)^{\eta_{\rm IA}}, \qquad (2)$$

where $C_1\rho_{\rm cr} = 0.0132, z_0 = 0.62$, and $G(z)$ represents the linear growth factor. The parameters $a_{\rm IA}$ and $\eta_{\rm IA}$ quantify the amplitude and redshift evolution of the IA signal, respectively. We adopt priors ranging from -5 to 5 for both $a_{\rm IA}$ and $\eta_{\rm IA}$.

To address uncertainties in the redshift distribution of galaxies in photometric surveys, we introduce photo-z bias parameters, Δ_z^i. These parameters shift the estimated redshift distributions $\hat{n}$ according to:

$$n^i(z) \to \hat{n}^i(z + [1 + \bar{z}^i]\Delta_z^i), \qquad (3)$$

where $\bar{z}^i$ denotes the mean redshift of the i-th tomographic bin. We assign Gaussian priors centered at zero with standard deviations of 0.002 for each of the five source bins, resulting in five photo-z bias parameters in total.

We parameterize uncertainties in measuring galaxy shapes through a multiplicative shear calibration bias. To account for this bias, we assign one parameter per source bin, totaling five parameters. During the inference stage, we model their impact on the cosmic shear correlation function as

$$\xi_{\pm}^{ij}(\theta) \to (1 + m^i)(1 + m^j)\xi_{\pm}^{ij}(\theta; m = 0). \qquad (4)$$

We adopt Gaussian priors centered at zero with a standard deviation of 0.005 for each of the five shear calibration parameters.

To compute the theoretical data vectors, we utilize the Cobaya-CosmoLike Joint Architecture (CoCoA).

3.3. *Gaussian Island Specifications*

For the outlier determination, we assume that the redshift distribution is described by

$$n(z) = (1-\alpha) * n_{fid}(z) + \alpha * n_{out}(z), \tag{5}$$

where $n_{fid}(z)$ is the redshift distribution without outliers, $n_{out}(z)$ represents the redshift distribution contribution from catastrophic outliers, and α is the outlier fraction. In a sample of N galaxies, each with a spectroscopic and photometric redshift, the outlier fraction is the fraction of N that falls within either of the islands described in Section 2.3.

In the Gaussian outlier model, we assume that

$$p_{\rm out}(z_{tr}, z_{ph}) = \frac{1}{\sqrt{(2\pi)^2|\mathbf{C}|}} \exp\Big[-\frac{1}{2}(\boldsymbol{z}-\boldsymbol{z}_0)^T\mathbf{C}^{-1}(\boldsymbol{z}-\boldsymbol{z}_0)\Big], \tag{6}$$

where $\boldsymbol{z} = (z_{tr}, z_{ph})$ and $\boldsymbol{z}_0$ defines the center of the Gaussian island. We further assume a diagonal covariance matrix of the redshifts,

$$\mathbf{C} = \begin{pmatrix} \sigma^2_{z,tr} & 0 \\ 0 & \sigma^2_{z,ph} \end{pmatrix}. \tag{7}$$

When we bin galaxies into a tomographic bin, we select galaxies with $z_{ph} \in [z_{lo}, z_{hi}]$. Therefore, the contribution to $n(z)$ of the outliers is given as

$$\begin{aligned} n_{\rm out}(z) &= \int_{z_{lo}}^{z_{hi}} dz_{ph} p_{\rm out}(z_{tr}, z_{ph}), &(8)\\ &= \frac{1}{\sqrt{2\pi}\sigma_{z,tr}} \exp\Big[-\frac{(z_{tr}-z_{tr,0})^2}{2\sigma^2_{z,tr}}\Big] &(9)\\ &\quad \times \int_{z_{lo}}^{z_{hi}} dz_{ph} \frac{1}{\sqrt{2\pi}\sigma_{z,ph}} \exp\Big[-\frac{(z_{ph}-z_{ph,0})^2}{2\sigma^2_{z,ph}}\Big] \\ &= \frac{\mathcal{A}(z_{ph,0}, z_{lo}, z_{hi})}{\sqrt{2\pi}\sigma_{z,tr}} \exp\Big[-\frac{(z_{tr}-z_{tr,0})^2}{2\sigma^2_{z,tr}}\Big], &(10)\end{aligned}$$

where,

$$\mathcal{A}(z_{ph,0}, z_{lo}, z_{hi}) = \frac{1}{2}\Big[\mathcal{E}(z_{hi}) - \mathcal{E}(z_{lo})\Big]. \tag{11}$$

Here,

$$\mathcal{E}(z) = \mathrm{erf}\Big[\frac{(z-z_{ph,0})}{\sqrt{2}\sigma_{z,ph}}\Big], \tag{12}$$

where erf is the error function.

4. RESULTS

In this section, we examine how catastrophic photometric redshift (photo-z) outliers influence cosmological parameter estimation in simulated LSST-Y1 data. By systematically introducing varying fractions and types of these outliers, we quantify their effects on key parameters, including Ω_m, the time evolution of dark energy (w), and S_8, and discuss the implications for next-generation large-scale surveys.

To evaluate the impact of outliers, we employ the Gaussian Island Model introduced in Section 3.3 to generate simulated data vectors with varying outlier fractions and distributions. For each scenario, we perform cosmological parameter inference using Markov Chain Monte Carlo (MCMC) sampling. At every step of the MCMC chain, we compute the posterior probability as described by Boruah et al. (2022, 2024), where

$$\mathcal{P}(\theta|d_{sim}) \;\propto\; \mathcal{L}(\theta|d_{sim})\mathcal{P}(\theta). \tag{13}$$

Here, the likelihood function - assumed to be Gaussian - is

$$log\mathcal{L}(\theta|d_{sim}) = -\frac{1}{2}[d_{model}(\theta) - d_{sim}]^T C^{-1}[d_{model}(\theta) - d_{sim}]. \tag{14}$$

Here, θ represents the cosmological and systematic parameters, and $\mathcal{P}(\theta)$ denotes the priors on these parameters. The simulated data vectors, d_{sim}, are computed at a fiducial point in parameter space. The statistical uncertainties, encapsulated in the covariance matrix C, for the data vectors in Equation 14 are calculated analytically using the CosmoLike software (Krause & Eifler 2017). This code computes the Gaussian covariance, connected non-Gaussian terms, and super-sample covariance components through an analytical framework. Additionally, the model data vectors, d_{model}, are computed as functions of the parameters θ.

In these analyses, we assume an outlier-free source redshift distribution ($n(z)$) within our model, while the simulated data vectors (d_{sim}) contain varying levels of outlier contamination. By comparing the resulting parameter inferences against those obtained from an uncontaminated baseline, we quantify how sensitive cosmological conclusions are to the presence and fraction of catastrophic photo-z outliers. The following subsections detail the observed parameter shifts under different outlier scenarios and identify the conditions most prone to significant biases.

4.1. *Fiducial and 1% Contamination*

In our impact study, we examine the effects of the false high-z and false low-z galaxies independently. By introducing outliers from only one island at a time, we isolate each island's influence on cosmological parameter estimation. This approach helps identify which type of catastrophic outlier contamination is more critical to address in future analyses.

We begin by analyzing the cosmological parameter constraints derived from an outlier-free data vector.

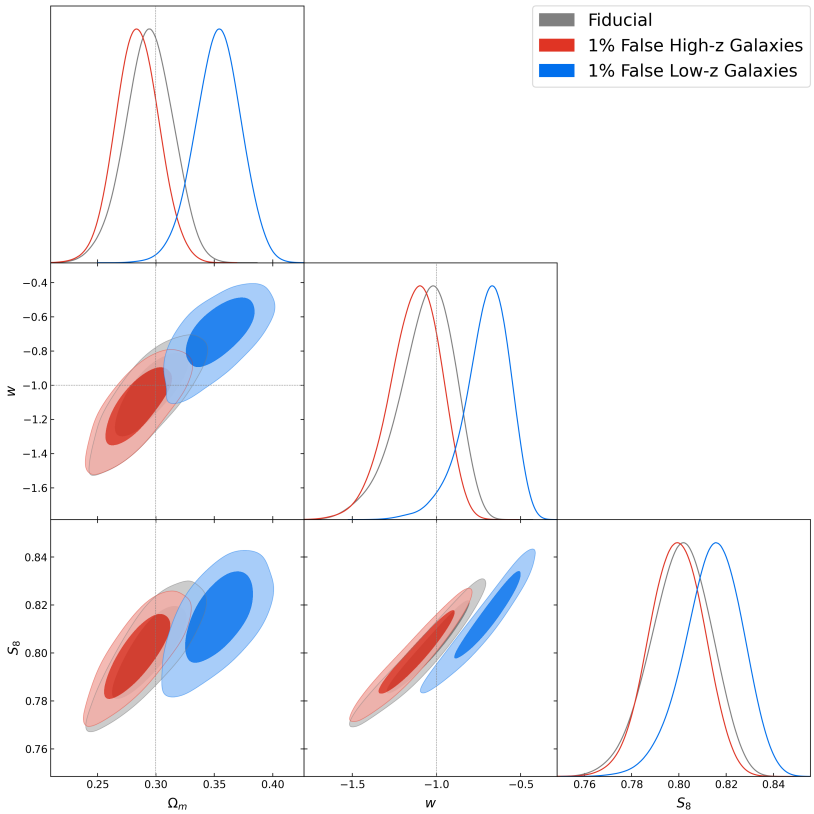

Figure 3. The distributions of Ω_m, w, and S_8 derived from 3 data vectors. The gray contours show the results for an outlier-free data vector. The red contours show the results for a data vector with 1% outliers consisting of only false high-z galaxies. The blue contours show the results for a data vector with 1% outliers consisting of only false low-z galaxies. The dashed lines indicate the fiducial values of each cosmological parameter, where applicable.

This serves as the fiducial model, representing the expected parameter constraints from an ideal LSST-Y1 survey without contamination from catastrophic outliers. As depicted in Figure 3, the gray contours represent the posterior distributions for Ω_m, w, and S_8. These results align closely with the fiducial values, indicating that our model accurately recovers the underlying cosmology in the absence of outliers.

Simulating a 1% contamination in our data vector of false high-z galaxies (red contours in Figure 3) leads to noticeable but minor shifts in the posterior distributions of the cosmological parameters Ω_m, w, and S_8. Specifically, the peaks of these parameters shift to lower values by 3.55%, 7.43%, and 0.32% respectively. These percentage changes are relatively small compared to the overall parameter uncertainties, and would likely pass the criteria for any cosmological survey.

Contrary to the false high-z galaxies, simulating a 1% contamination of false low-z galaxies (blue contours in Figure 3) results in more substantial shifts in the opposite direction. The cosmological parameters Ω_m, w, and S_8 shift to larger values, with their peaks moving by 20.49%, 34.21%, and 1.70%, respectively.

These shifts are more pronounced than those caused by false high-z galaxies, indicating that false low-z galaxies have a more significant impact on cosmological parameter estimation. For instance, a 20.49% increase in Ω_m could lead to a considerable overestimation of the matter density, while the corresponding shifts in w and S_8 might affect our interpretations of dark energy and matter clustering differently.

4.2. *Analysis of Varying Outlier Fractions*

To further understand the relationship between outlier fractions and cosmological parameters, we analyze multiple scenarios with varying levels of contamination from both false high-z and false low-z galaxies. Figure 4 illustrates the mean parameter values and their uncertainties across these different outlier fractions.

4.2.1. *Matter Density*

The matter density parameter, Ω_m, exhibits a clear sensitivity to the contamination from low photo-z outliers. As the fraction of these outliers increases, Ω_m deviates progressively further from its fiducial value, indicating a significant bias in its estimation. Concurrently, the uncertainty associated with Ω_m widens with higher

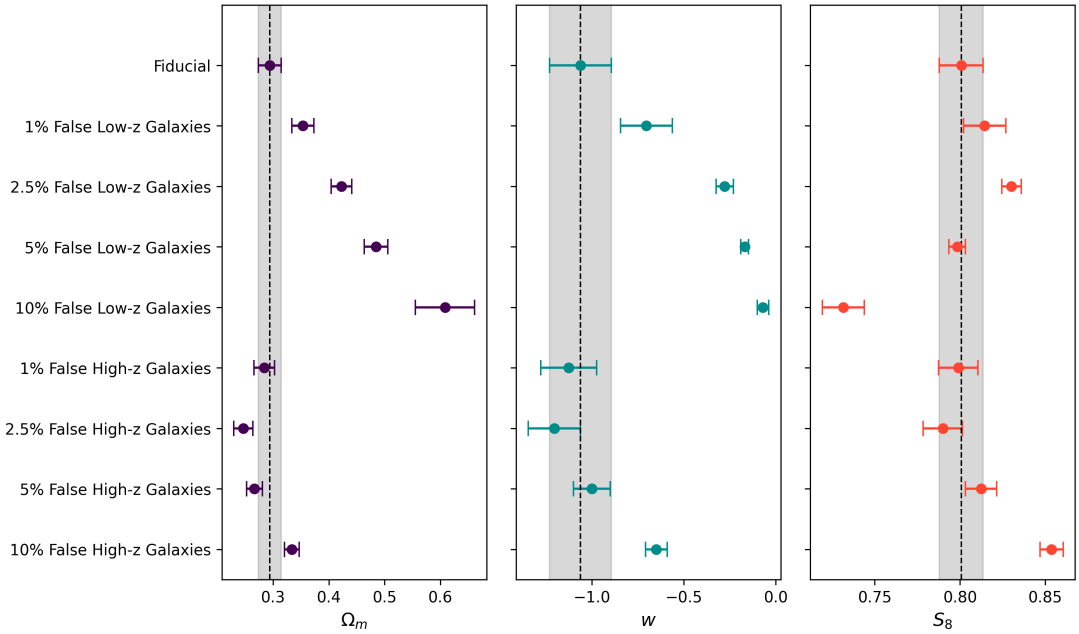

Figure 4. The constraints of Ω_m, w, and S_8 derived from 3 data vectors. The points represent the mean values among all 4 chains, and the error bars are the standard deviations. The first row shows the results for an outlier-free data vector. The next 4 rows show the results for data vectors with various outlier percentages consisting of only the false low-z galaxies. The final 4 rows show the results for data vectors with various outlier percentages consisting of only the false high-z galaxies. The dashed line and gray region highlight the means and standard deviations of the fiducial data vector, respectively.

outlier percentages, reflecting reduced precision in the parameter constraints.

In stark contrast, the introduction of high photo-z outliers has a minimal impact on Ω_m. Even at elevated contamination levels, the estimated values of Ω_m remain closely aligned with the fiducial value, and the corresponding error bars show little to no expansion. This suggests that Ω_m is predominantly influenced by low photo-z outliers, while high photo-z contaminants do not substantially affect its determination.

4.2.2. *Equation of State Parameter*

The equation of state parameter, w, exhibits a nuanced response to photo-z outlier contamination, paralleling some aspects of the behavior observed for the matter density parameter.

Specifically, when low photo-z outliers are introduced, the uncertainty in w initially starts at a relatively large value. However, as the fraction of these outliers increases, the uncertainty in w progressively diminishes. This reduction in the error bar suggests that higher levels of low photo-z contamination may, counterintuitively, lead to tighter constraints on w, although this does not necessarily imply an improvement in accuracy.

Moreover, the degree of deviation of w from its fiducial value appears to decrease as the outlier fraction increases. Each incremental addition of low photo-z outliers results in a smaller increase in the estimated value of w, indicating a diminishing sensitivity to further contamination.

On the other hand, the introduction of high photo-z has a negligible effect on the estimation of w. Contamination levels of 1%, 2.5%, and 5% from the high photo-z island result in w estimates that remain well within the error bars of the fiducial value.

4.2.3. *Structure Formation*

The amplitude of matter fluctuations, characterized by the parameter S_8, displays a particularly complex and intriguing response to photo-z outliers.

When low photo-z outliers are introduced, the initial impact on S_8 mirrors that of the equation of state parameter w. However, as the contamination level increases to 5%, the deviation from the fiducial value diminishes, bringing the S_8 estimate nearly back in line with the expected values. This reversal indicates that moderate levels of low photo-Z contamination may inadvertently correct some of the initial biases introduced at lower contamination levels. Furthermore, the reversal continues through to 10%, where the estimated value is significantly lower than the fiducial value.

Conversely, high photo-z outliers affect S_8 in a manner consistent with its impact on other cosmological parameters. Significant deviations from the fiducial S_8 value are not observed until the contamination level reaches 10%. Lower levels of high photo-z contamination do not

produce substantial shifts in S_8, allowing the parameter to remain within the expected range of the fiducial model.

5. CONCLUSIONS

This thesis set out to understand and mitigate the impact of catastrophic photometric redshift (photo-z) outliers on cosmological parameter estimation in next-generation large-scale surveys, with a focus on the Vera C. Rubin Observatory's Legacy Survey of Space and Time (LSST). As the LSST seeks to achieve unprecedented precision in mapping the large-scale structure of the universe, it is critical to ensure that systematics—particularly those arising from inaccurate redshift estimates—do not bias our interpretation of dark matter, dark energy, and cosmic structure formation.

5.1. *Impact Study Summary*

The comprehensive analysis of varying outlier fractions from both the false high-z and false low-z galaxies elucidates the differential impact these contaminants have on key cosmological parameters. We find that the false low-z galaxies are inherently more challenging to address and mitigate compared to their false high-z counterparts. Parameters like Ω_m and w are highly sensitive to false low-z galaxy contamination, meaning even small fractions of these outliers can introduce significant biases. This necessitates more rigorous strategies for their detection and correction.

In contrast, false high-z galaxies only significantly affect cosmological parameters at higher contamination levels, and their impact is more predictable and less severe at lower fractions. This relative insensitivity makes them somewhat easier to manage, as their influence can be tolerated up to a certain threshold without critically biasing the results.

Given the pronounced effects of false low-z galaxies on crucial cosmological parameters, it is imperative to accurately estimate their fractions within the dataset or model them in our cosmological analyses. Precise knowledge of the false low-z outlier fraction is essential for ensuring that the biases introduced by these outliers are correctly accounted for, thereby preserving the integrity of parameter estimates.

5.2. *Limitations and Assumptions*

The Gaussian Island Model employed here provides a convenient framework to capture outlier behavior, but it inevitably simplifies reality. In practice, outlier distributions may be more complex or exhibit non-Gaussian tails. Further, we assumed that the fraction and distributions of outliers are known or could be directly varied; in real analyses, these fractions will carry their own uncertainties. Additionally, we focused on weak lensing alone and did not include baryonic feedback or other subtle astrophysical effects that may become relevant at small scales.

5.3. *Future Work*

Future endeavors should refine the outlier model by allowing for more complex distributions or multiple, overlapping outlier populations. Incorporating joint analyses with galaxy clustering, CMB lensing, or other cosmological probes could help break degeneracies introduced by photo-z errors. Additionally, targeted spectroscopic campaigns and enhanced training sets for photo-z estimation algorithms are crucial for accurately measuring and reducing outlier fractions. In particular, catastrophic photo-z outliers can be mitigated by expanding the spectroscopic dataset, making missions like the Roman Space Telescope (Spergel et al. 2015) and DESI (DESI Collaboration et al. 2016) synergistic partners of LSST. As LSST progresses, iterative calibration approaches, where early data is utilized to refine redshift estimates for subsequent epochs, may prove essential for improving overall measurement accuracy and reliability.

5.4. *Final Takeaways*

In this thesis, we have demonstrated that catastrophic photo-z outliers pose a serious challenge for interpreting weak lensing measurements in LSST. Our findings show that knowledge of the fraction and nature of these outliers is crucial; without it, even a Year-1 analysis risks biased cosmological conclusions. By highlighting the sensitivity of key parameters to outlier populations, this work provides valuable guidance for survey strategies and calibration efforts. As the cosmological community prepares for the era of precision cosmology, the insights presented here will help ensure that we fully harness the potential of surveys like LSST, advancing our understanding of the fundamental components and evolution of the universe.

ACKNOWLEDGMENT

This work is supported by the Department of Energy HEP-AI program grant DE-SC0023892 and the Cosmic Frontier program grant DE-SC0020215. The simulations in this paper use High Performance Computing (HPC) resources supported by the University of Arizona TRIF, UITS, and RDI and maintained by the UA Research Technologies department.

REFERENCES

Abbott, T. M. C., Aguena, M., Alarcon, A., et al. 2022, Phys. Rev. D, 105, 023520, doi: 10.1103/PhysRevD.105.023520

Abdalla, E., Abellán, G. F., Aboubrahim, A., et al. 2022, Journal of High Energy Astrophysics, 34, 49–211, doi: 10.1016/j.jheap.2022.04.002

Bernstein, G., & Huterer, D. 2010, Monthly Notices of the Royal Astronomical Society, 401, 1399, doi: 10.1111/j.1365-2966.2009.15748.x

Boruah, S. S., Eifler, T., Miranda, V., & Krishanth, P. M. S. 2022, Monthly Notices of the Royal Astronomical Society, 518, 4818–4831, doi: 10.1093/mnras/stac3417

Boruah, S. S., Eifler, T., Miranda, V., et al. 2024. https://arxiv.org/abs/2403.11797

Bridle, S., & King, L. 2007, New Journal of Physics, 9, 444, doi: 10.1088/1367-2630/9/12/444

DESI Collaboration, Aghamousa, A., Aguilar, J., et al. 2016, arXiv e-prints, arXiv:1611.00036, doi: 10.48550/arXiv.1611.00036

Fang, X., Eifler, T., & Krause, E. 2020, Monthly Notices of the Royal Astronomical Society, 497, 2699, doi: 10.1093/mnras/staa1726

Fang, X., Eifler, T., Schaan, E., et al. 2021, Monthly Notices of the Royal Astronomical Society, 509, 5721, doi: 10.1093/mnras/stab3410

Graham, M. L., Connolly, A. J., Željko Ivezić, et al. 2018, The Astronomical Journal, 155, 1, doi: 10.3847/1538-3881/aa99d4

Graham, M. L., Connolly, A. J., Wang, W., et al. 2020, The Astronomical Journal, 159, 258, doi: 10.3847/1538-3881/ab8a43

Heymans, Catherine, Tröster, Tilman, Asgari, Marika, et al. 2021, AA, 646, A140, doi: 10.1051/0004-6361/202039063

Ivezić, Ž., Kahn, S. M., Tyson, J. A., et al. 2019, ApJ, 873, 111, doi: 10.3847/1538-4357/ab042c

Krause, E., & Eifler, T. 2017, Monthly Notices of the Royal Astronomical Society, 470, 2100, doi: 10.1093/mnras/stx1261

MacCrann, N., Becker, M. R., McCullough, J., et al. 2021, Monthly Notices of the Royal Astronomical Society, 509, 3371–3394, doi: 10.1093/mnras/stab2870

Mandelbaum, R. 2018, Annual Review of Astronomy and Astrophysics, 56, 393–433, doi: 10.1146/annurev-astro-081817-051928

Poulin, V., Bernal, J. L., Kovetz, E. D., & Kamionkowski, M. 2023, Physical Review D, 107, doi: 10.1103/physrevd.107.123538

Schaan, E., Ferraro, S., & Seljak, U. 2020, Journal of Cosmology and Astroparticle Physics, 2020, 001–001, doi: 10.1088/1475-7516/2020/12/001

Smail, I., Hogg, D. W., Yan, L., & Cohen, J. G. 1995, ApJL, 449, L105, doi: 10.1086/309647

Spergel, D., Gehrels, N., Baltay, C., et al. 2015, arXiv e-prints, arXiv:1503.03757, doi: 10.48550/arXiv.1503.03757

Sun, L., Fan, Z.-H., Tao, C., et al. 2009, The Astrophysical Journal, 699, 958–967, doi: 10.1088/0004-637x/699/2/958

The LSST Dark Energy Science Collaboration, Mandelbaum, R., Eifler, T., et al. 2018, arXiv e-prints, arXiv:1809.01669, doi: 10.48550/arXiv.1809.01669